Climate Dynamics (2019) 52:7537–7552
https://doi.org/10.1007/s00382-018-4290-4

On the variety of coastal El Niño events

Zeng-Zhen Hu[1] · Bohua Huang[2] · Jieshun Zhu[1,3] · Arun Kumar[1] · Michael J. McPhaden[4]

Received: 15 January 2018 / Accepted: 18 May 2018 / Published online: 6 June 2018

Abstract
We examine the connection between interannual anomalies of sea surface temperature (SST) in the central and far-eastern equatorial Pacific associated with basin-scale and coastal El Niños. Variations of the SST anomalies in these two regions are largely coherent, meaning coastal El Niños mostly occur together with the commonly studied basin-scale El Niños. Of particular interest for this study though is the understanding of the coastal El Niños that are not accompanied by basin-scale El Niños or that follow basin-scale El Niños. Such coastal El Niños can have catastrophic societal consequences in western South America. We identify seven coastal El Niños during 1979–2017, namely 1983, 1987, 1998, 2008, 2014, 2015, and 2017. These coastal El Niños are driven by different mechanisms. The coastal El Niños in 1983, 1987 and 1998 occurred after basin-scale El Niños. A unique feature of such extreme basin-scale El Niños like in 1982–1983, 1986–1987, and 1997–1998 is an equatorially centered intertropical convergence zone during its decaying phase. As a result, positive SST anomalies persist, and sometimes even strengthen, in the eastern Pacific in the subsequent boreal spring/early-summer, leading to coastal El Niños. The coastal El Niños in 2014 and 2015 on the other hand resulted from westerly wind bursts in the western Pacific that forced downwelling Kelvin waves and a thermocline depression in the far eastern Pacific. The formation of coastal El Niños in 2008 and 2017 were associated with westerly surface wind anomalies in the eastern equatorial Pacific and largely driven by ocean surface heat flux anomalies. These two coastal El Niños occur during the warm phase of the seasonal cycle, so that warm SSTs are amplified and/or the warm season is extended along the west coast of South America. Thus, there is a wide variety of the coastal El Niños in terms of evolution, mechanism, and timing.

1 Introduction

El Niño–Southern Oscillation (ENSO) originates in the tropical Pacific and is the strongest year-to-year fluctuation of the climate system on the earth. It is also the largest source of predictability in global climate on seasonal-to-interannual time scales (National Research Council 2010). Originally, El Niño was referred to as anomalous warming along the Peru-Ecuador coast every few years, which sometimes resulted in catastrophic rain and adverse impacts on regional ecology (see the review by Wyrtki 1975). Only later was it recognized that most El Niños (the warm phase of ENSO) and La Niñas (the cold phase of ENSO) are Pacific basin-wide phenomena associated with broad scale ocean-atmosphere interactions that have significant global climate impacts (Rasmusson and Carpenter 1982; Deser and Wallace 1987; Davey et al. 2014; McPhaden et al. 2006).

Rasmusson and Carpenter (1982) found that the sea surface temperature (SST) warming near the South America coast usually preceded that in the central equatorial Pacific during the El Niños from the 1950 to 1970s so that coastal

This paper is a contribution to the special collection on ENSO Diversity. The special collection aims at improving understanding of the origin, evolution, and impacts of ENSO events that differ in amplitude and spatial patterns, in both observational and modeling contexts, and in the current as well as future climate scenarios. This special collection is coordinated by Antonietta Capotondi, Eric Guilyardi, Ben Kirtman and Sang-Wook Yeh.

✉ Zeng-Zhen Hu
Zeng-Zhen.Hu@NOAA.GOV

[1] Climate Prediction Center, NCEP/NWS/NOAA, 5830 University Research Court, College Park, MD 20740, USA

[2] COLA and Department of Atmospheric, Oceanic, and Earth Sciences, College of Science, George Mason University, Fairfax, VA, USA

[3] Earth System Science Interdisciplinary Center, University of Maryland, College Park, MD 20740, USA

[4] NOAA/Pacific Marine Environment Laboratory, Seattle, WA 98115, USA

SST anomalies (SSTAs) could serve as a precursor to the subsequent basin-scale warm events. However, this relationship did not hold in the subsequent 1982–1983 strong El Niño (Rasmusson and Wallace 1983) and does not seem to be prominent in the warm events since. Furthermore, coastal El Niños sometimes also occur independent of the basin-scale El Niños with SSTA confined in the far-eastern tropical Pacific near the southern American coast (Takahashi and Martínez 2018). To distinguish such types of coastal El Niños, which can have catastrophic effects in western South America (Deser and Wallace 1987; Sanabria et al. 2018), we refer to the conventional El Niño as basin-scale El Niños. These basin-scale El Niños encompass a variety of different flavors as described in publications (e.g., Larkin and Harrison 2005; Ashok et al. 2007; Kug et al. 2009; Kao and Yu 2009; Hu et al. 2012; Capotondi et al. 2015; Wang et al. 2018).

The recent extreme warming along the South American coast during boreal spring 2017 (Fig. 1a–c) is one type of coastal El Niño event (Garreaud 2018). The warming commenced in boreal winter of 2016–2017, peaked in March 2017, and decayed in May. This coastal warm event led to serious regional weather and climate-related disasters. According to Frase (2017), torrential rains pummeled Peru's northern coastal desert in February and March 2017, triggering floods and landslides that killed at least 113 people and destroyed about 40,000 homes. Also, most of the water distribution systems in the region collapsed, causing drinking water shortages. A similar scenario happened in 1925 with strong warm SSTAs confined in the coastal region of South America during boreal spring (Fig. 1e–g), which also caused loss of life and property in the region (Takahashi and Martínez 2018). Nevertheless, the intense coastal warming in 1925 developed in a largely cold background of the Pacific basin, instead of a warm state as in 2017 (Fig. 1). Interestingly, the coastal El Niño eventually evolved into a strong basin-scale El Niño in 1925, but was followed by a basin-scale La Niña in 2017 (Fig. 1d, h).

In contrast with the extensive and systematical research about the basin-scale El Niño (Philander 1990; Sarachik and

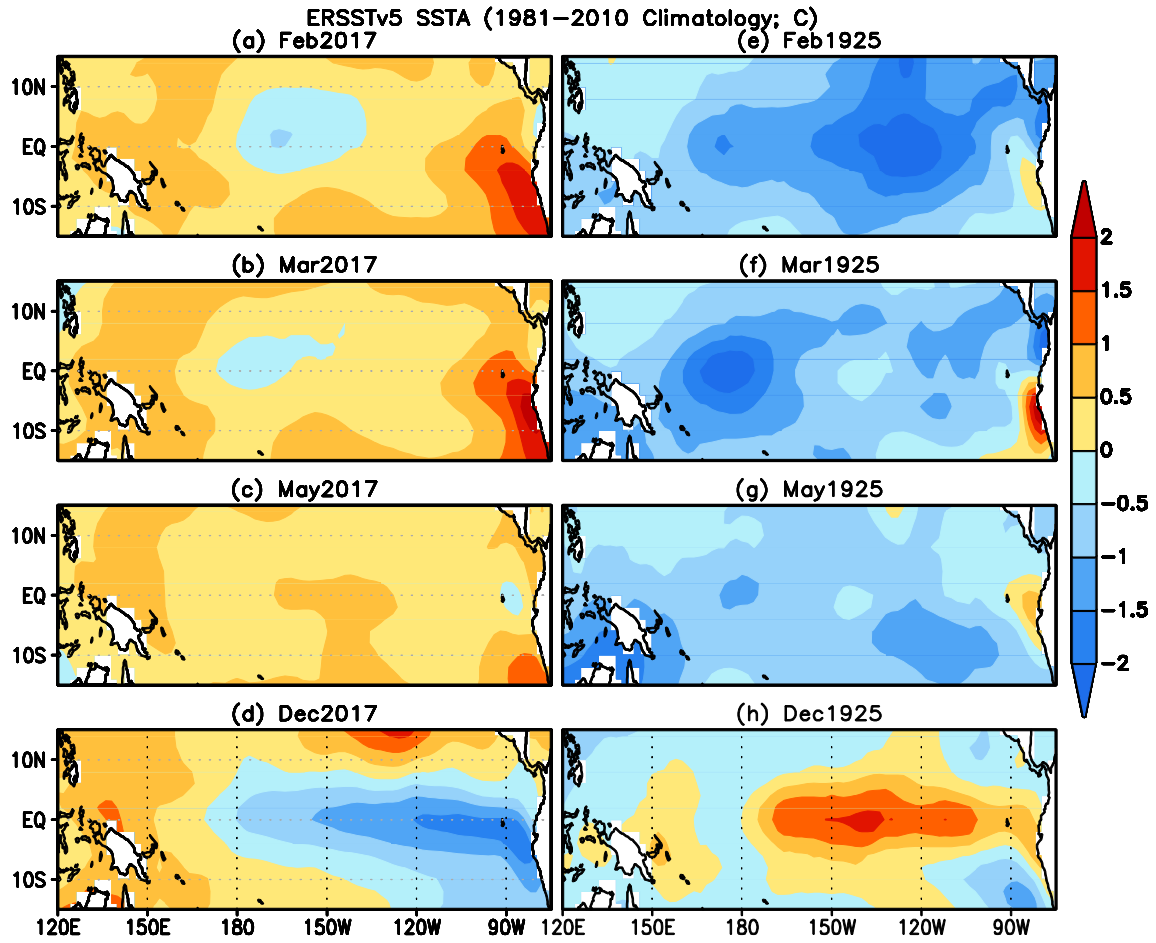

Fig. 1 SSTAs in **a** February 2017, **b** March 2017, **c** May 2017, **d** December 2017, and **e** February 1925, **f** March 1925, **g** May 1925, and **h** December 1925. The unit is °C

Cane 2010), the knowledge and research in understanding aspects of coastal El Niño are very limited. Recently, Takahashi and Martínez (2018) examined the coastal El Niño event in early 1925 based on limited *in situ* observations. As seen in Fig. 1, this strong coastal El Niño was characterized by warm conditions in the far-eastern Pacific, but cool conditions in the central tropical Pacific. That is in contrast to coastal warming after the peak phases of the extreme El Niño events in 1982–1983 and 1997–1998. In these two events, strong positive SSTAs were also observed in both the central and eastern tropical Pacific. Takahashi and Martínez (2018) argued that downwelling equatorial Kevin waves had little role in initiating the coastal warming in 1925. In fact, the coastal warming in 1925 was associated with an abrupt onset of strong northerly winds across the equator and the strengthening/weakening of the intertropical convergence zones (ITCZ) south/north of the equator. They suggested that the coupled ocean–atmosphere feedback dynamics associated with southward shift of ITCZs, enhanced convergence along the ITCZ (see their Fig. 8) and enlarged north–south SSTA asymmetry in the far-eastern Pacific (see their Fig. 5) produced the coastal El Niño event in 1925. However, it is unclear whether the onset of strong northerly winds across the equator and southward shift of ITCZ are a connection or causal relationship.

The catastrophic impacts of coastal El Niños on life and property, as well as our limited knowledge currently about its physical mechanisms, call for further studies about the physical processes behind these events, that is the focus of this paper. The rest of the paper is organized as follows. The data used in this work are introduced in Sect. 2. Section 3 shows the connection of SSTAs in the central and far eastern equatorial Pacific and its interdecadal and seasonal variations. In Sect. 4, criteria to identify a coastal El Niño are proposed. Various mechanisms for the evolution of coastal El Niños are examined in Sect. 5. A summary and discussion are given in Sect. 6.

2 Data

Monthly mean SSTs are from version 5 of the Extended Reconstructed SST (ERSSTv5) dataset on a $2^\circ \times 2^\circ$ grid during January 1854–December 2017, which is based on reconstruction from empirical orthogonal functions (EOFs). While ERSSTv5 is unable to distinguish some regional and small-scale anomalies because of the inherent EOF smoothing (Huang et al. 2017), it captues the essential feature we are interested in. The Niño1 + 2 and Niño3.4 indices are defined as the averaged SSTA in the regions 10°S–0°N, 90°W–80°W and 5°S–5°N, 170°W–120°W, respectively. This long SST time-series is used to analyze the relationship between SST variations in the Niño3.4 and Niño1 + 2 regions.

Monthly and pentad mean surface wind stresses during January 1979–December 2017 are from the NCEP/DOE reanalysis (Kanamitsu et al. 2002). Monthly and pentad mean of depth of the 20 °C isotherm (D20), SST, surface heat flux, and vertical velocity (w) from the Global Ocean Data Assimilation System (GODAS; Behringer 2005) during January 1979–December 2017 are also analyzed. Monthly mean outgoing long wave radiation (OLR) and analyzed precipitation data on a $2.5^\circ \times 2.5^\circ$ grid are from Liebmann and Smith (1996) and Xie and Arkin (1997), respectively.

3 Connection of SSTAs in the central and far-eastern equatorial Pacific

First, we analyze the lead-lag connections of SSTAs in the central and far-eastern equatorial Pacific, which are represented by the Niño3.4 and Niño1 + 2 indices, respectively (Fig. 2). We note that the two indices are positively correlated (Fig. 2), implying coherent variation of SSTAs in the central and far-eastern equatorial Pacific. In other words, coastal and basin-scale warming/cooling (El Niño/La Niña) occur together most of the time. The maximum correlation occurs when the Niño3.4 index lags the Niño1 + 2 index by 1–2 months, suggesting that statistically SST variation in the far-eastern equatorial Pacific occurs slightly earlier than that in the central equatorial Pacific, consistent with the composite analysis by Rasmusson and Wallace (1983) based on six El Niños in the 1950–1970s.

The lead-lag relationship of SSTAs in the central and far-eastern equatorial Pacific also experienced some interdecadal variations (Fig. 3). For example, during 1870–1980, the maximum correlations are present when the Niño3.4 index lags the Niño1 + 2 index by 1–3 months, implying a westward propagation as indicated in Rasmusson and Carpenter (1982). Since late 1970s, the maximum correlations are present at 0 month lead, suggesting that a change of the zonal propagation direction of SSTAs after about 1980 (e.g., Wang 1995; Zhu et al. 2011). McPhaden and Zhang (2009) highlighted the asymmetry in zonal phase propagation between El Niño and La Niña SSTAs after 1980. In particular, the phase propagation of El Niño associated SSTAs along the equator changed from westward to eastward after mid- to late-1970s climate regime shift in the Pacific. However, the direction of propagation of La Niña associated SSTAs did not change after the mid- to late-1970s. Instead, the La Niña associated SSTAs continued to exhibit westward phase propagation along the equator. Such asymmetry of the phase propagation between El Niño and La Niña associated SSTA

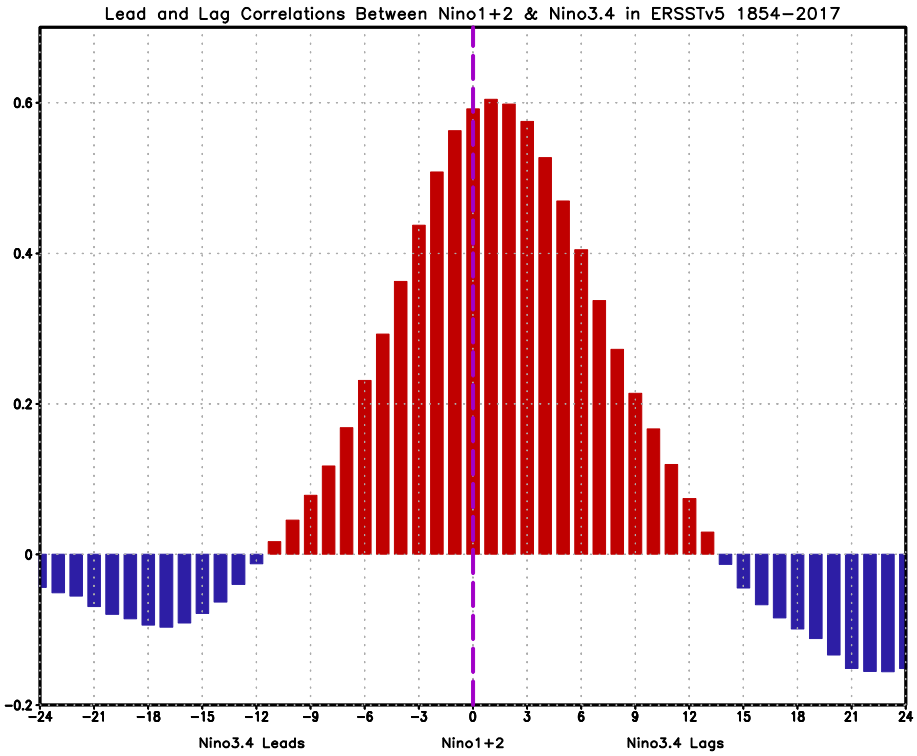

Fig. 2 Lead and lag correlations between the Niño3.4 and Niño1 + 2 indices. The negative (positive) numbers in the *x*-axis represent the number of months that the Niño3.4 index leads (lags) the Niño1 + 2 index

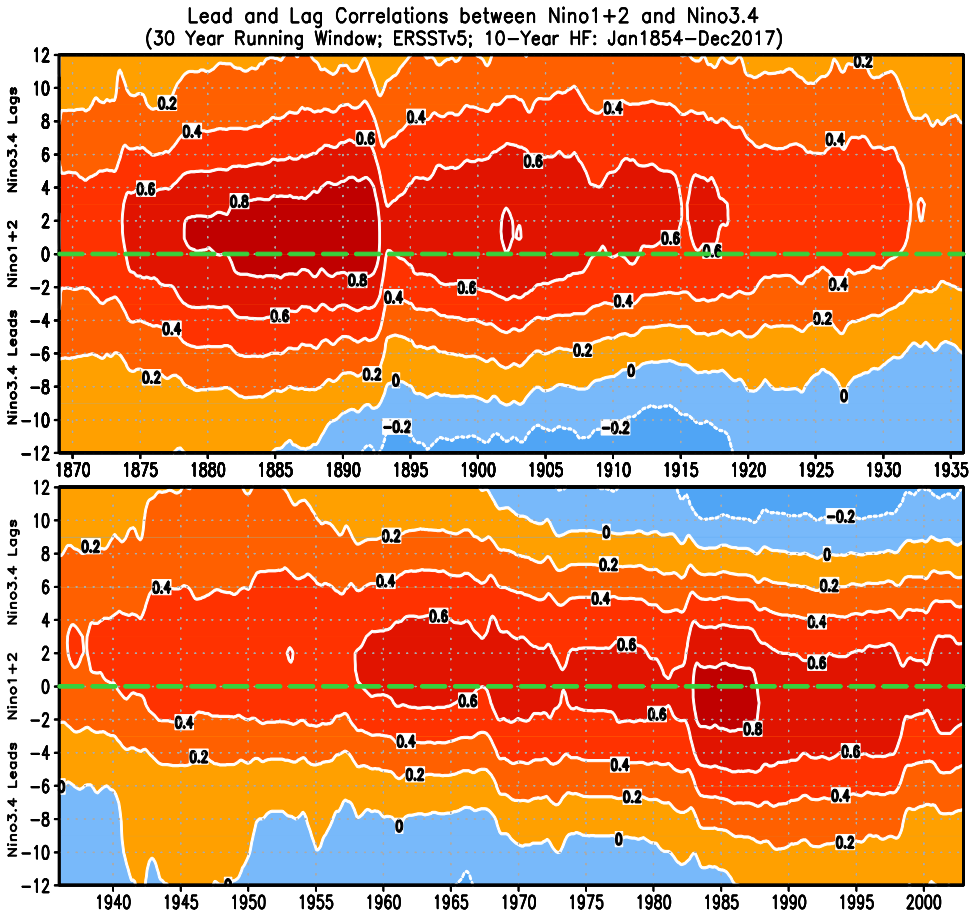

Fig. 3 Lead and lag correlations between the Niño3.4 and Niño1 + 2 indices with 30 years running window. The data are 10-year high-pass filtered. The negative (positive) numbers in the *y*-axis represent the number of months that the Niño3.4 index leads (lags) the Niño1 + 2 index

is consistent with the maximum lead-lag correlations occurring at 0-month lead-lag after about 1980.

In addition to interdecadal variation of the lead-lag time, the correlation amplitudes vary with time. For example, the correlations are stronger during 1875–1915 and since 1960, but weaker during 1920–1960 (Fig. 3). Such amplitude change of the correlation may be associated with interdecadal variations in ENSO intensity (D'Arrigo et al. 2005) or character (e.g. Ashok et al. 2007; McPhaden 2012). Interestingly, the lead-lag correlations vary with calendar months as well (Fig. 4). Statistically, the correlations are larger during August–January than other months. With the progression from late boreal spring to winter for the Niño1 + 2 index, the lead time of the Niño1 + 2 index to the Niño3.4 index reduces from 7 to 8 months to 0 month. That implies that the variability of SSTA in the Niño1 + 2 region precedes that in the Niño3.4 region mainly in the development phases of ENSO and there is little propagation of SSTAs during the peak phase of ENSO, consistent with the Rasmusson and Carpenter (1982) composites. Note also that in boreal winter there is tendency for the Niño3.4 index to lead the Niño1 + 2 index.

4 Definition of coastal El Niño event

According to L'Heureux et al. (2017), Comité encargado del Estudio Nacional del Fenómeno El Niño (ENFEN Committee, Peru) uses the following criteria to define a coastal El Niño (La Niña): 3-month running-mean Niño1 + 2 SST index is above (below) 0.4 °C (− 1.0 °C) for at least three consecutive months. In the present work, the analysis is focused on those coastal El Niños that do not occur simultaneously with basin-scale El Niños. To exclude coastal warming events co-existing with basin-scale El Niños, we remove the Niño3.4 related variability from the Niño1 + 2 SST index by subtracting it with a linear regression fit onto the Niño3.4 index. The residual time series is referred to as the ENSO-adjusted Niño1 + 2 index (see line in Fig. 5). In the subsequent analysis, as our purpose is to study the mechanisms for the coastal El Niños, the analysis period is limited to after 1979 when the data sets documenting the sub-surface ocean variability are available.

We note that in the ENSO-adjusted Niño1 + 2 index, only the part of the signal linearly related to the contemporary ENSO state is removed. It may have some remaining lead/lag correlations with the Niño3.4 index. Moreover, any nonlinearity in the relationship (that is expected to be strong for major El Niños, see Jin et al. 2003; An and Jin 2004) may still be present, including some prominent asymmetric features between El Niño and La Niña (Kumar and Hoerling

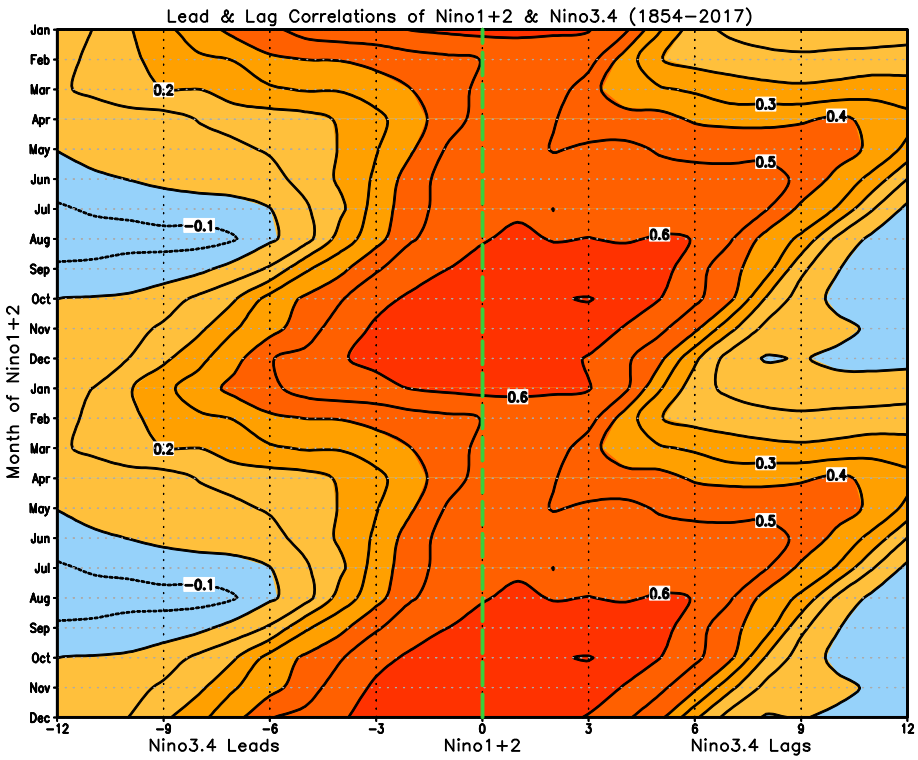

Fig. 4 Month dependence of lead and lag correlations between the Niño3.4 and Niño1 + 2 indices in 1854–2017. The negative (positive) numbers in the *x*-axis represent the number of months that the Niño3.4 index leads (lags) the Niño1 + 2 index. The *y*-axis is the months of the Niño1 + 2 index, and it spans 24 months

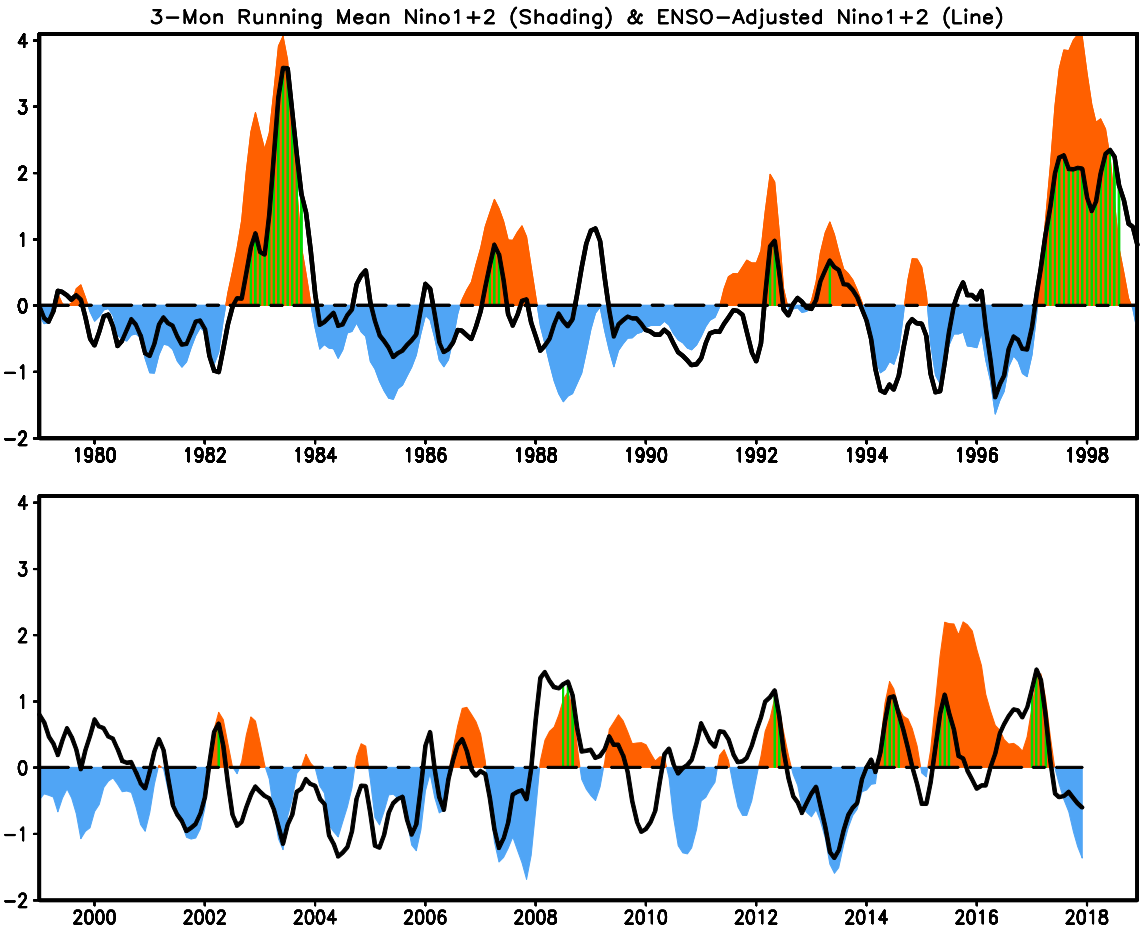

Fig. 5 Time series of 3-month running mean of Niño1 + 2 indices (shading) and ENSO-adjusted Niño1 + 2 indices (curve) in January 1979–December 2017. The bars represent that both the Niño1 + 2 index is equal to or larger than 0.8 °C and the ENSO-adjusted Niño1 + 2 index is equal to or larger than is 0.6 °C. The standard deviation is 1.1 °C for Niño1 + 2 index, 0.8 °C for ENSO-adjusted Niño1 + 2 index, 0.8 °C for Niño1 + 2 index without 1982–1983 and 1997–1998, and 0.6 °C for ENSO-adjusted Niño1 + 2 index without 1982–1983 and 1997–1998, respectively

1997; Yu and Kim 2011). For example, SSTAs in the tropical Pacific associated with El Niño and La Niña years are asymmetric in terms of their meridional extent (Zhang et al. 2009), amplitude (Hoerling et al. 1997), zonal phase propagation (McPhaden and Zhang 2009), and associated recharge/discharge processes (Hu et al. 2014, 2017).

On the other hand, we argue that this procedure substantially reduces the coastal SSTAs that are simultaneously and linearly related to basin-scale El Niños. To examine effectiveness of the ENSO-adjusted SSTAs in reducing the basin-scale ENSO associated SSTAs, Fig. 6 displays the raw SSTAs along the equator (left panel) and ENSO-adjusted SSTAs (by removing linear regression part of SSTAs associated with Niño3.4 from the raw SSTAs) (right panel). Clearly, the main SSTAs in the central and eastern equatorial Pacific disappear, with significant SSTAs present only in the far eastern Pacific and along the American coast. For extreme El Niños, SSTAs along the American coast (the Niño1 + 2 region), which are present simultaneously with extreme basin-scale El Niños, are largely removed in 1982 and 2015, and greatly reduced in 1997. Thus, we suggest that the SSTAs associated with basin-scale El Niños can be effectively removed through the linear regression fitting.

To distinguish the coastally confined warm/cold events from those co-occurring with basin-scale ENSO events, we propose a new approach. First, we exclude the extreme basin-scale El Niño events of 1982–1983 and 1997–1998 to avoid their overshadowing of other weaker coastal El Niño events. Then the standard deviations (STDs) of the Niño1 + 2 index and the ENSO-adjusted Niño1 + 2 index are calculated (Fig. 5). The correlation between the Niño1 + 2 index and the ENSO-adjusted Niño1 + 2 index reduces from 0.74 for all months to 0.58 for the months excluding January 1982–December 1983 and January 1997–December 1998 (Fig. 7). All the correlations are significant at the 99.9% level using the t-test, suggesting that a large fraction

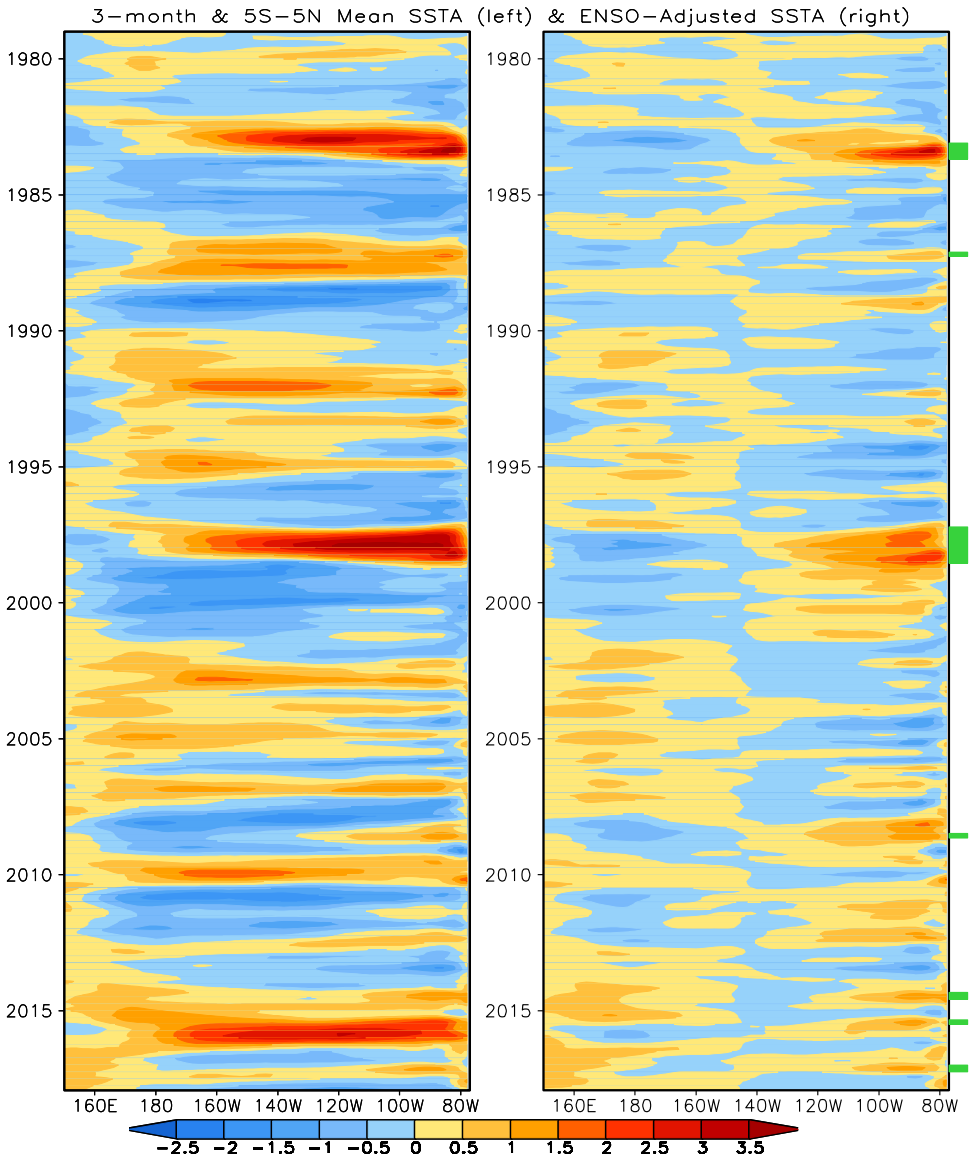

Fig. 6 Time and longitude evolution of 3-month running mean SSTAs (left) and ENSO-adjusted SSTAs (right) averaged in 5°S–5°N. The green rectangles in right side represent the duration of coastal El Niños defined in this work. The unit is °C

of SST variability in the Niño1 + 2 region is not linearly connected with basin-scale El Niños.

We define a coastal El Niño event when both the 3-month running mean Niño1 + 2 index is equal to or larger than one STD (0.8 °C) and ENSO-adjusted 3-month running mean Niño1 + 2 index is equal to or larger than one STD (0.6 °C) with anomalies of this magnitude persisting for at least three consecutive overlapping seasons. Following this definition, there are seven coastal El Niños during 1979–2017 (Fig. 8): 1983 (March–October 1983), 1987 (March–May 1987), 1998 (April 1997–August 1998), 2008 (July–September 2008), 2014 (May–August 2014), 2015 (May–July 2015), and 2017 (January-April 2017) (Fig. 5). The duration of the seven coastal El Niños ranges from 3 months (1987, 2008, 2015) to 17 months (1998) as evident in Fig. 6 (rectangles on right side) and Fig. 8 (bars).

5 Various mechanisms of generating Coastal El Niñoñ

The evolution of the Niño3.4 index in the seven coastal El Niño years is varies (Fig. 8, dashed line). For example, Niño3.4 decreases from large positive (strong basin-scale El Niño) to negative in 1983 and 1998 (Fig. 8a, c), but persists with large positive values in 1987 (Fig. 8b). For 2008 (Fig. 8d), Niño3.4 increases from large negative (a basin-scale La Niña) to near neutral. In 2014 and 2017 (Fig. 8e, g), the Niño3.4 index fluctuate around zero with small amplitude variations. The Niño3.4 index shows a strong increase in 2015 (Fig. 8f), that is associated with the development of the extreme basin-scale El Niño in 2015–2016 (Huang et al. 2016; L'Heureux et al. 2017).

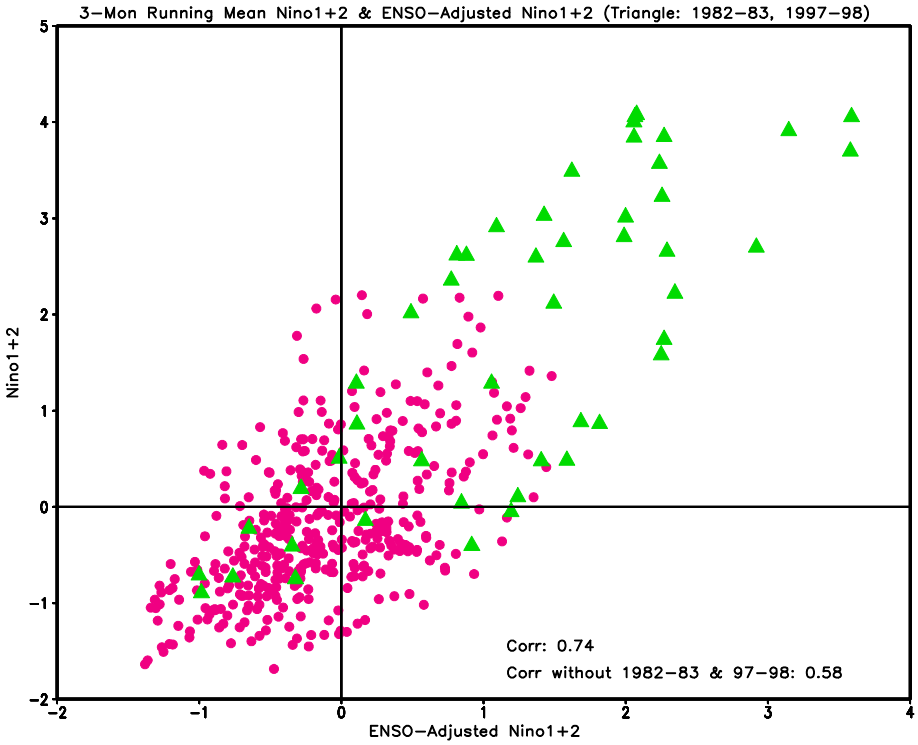

Fig. 7 Scatter of 3-month mean Niño1 + 2 (*y*-axis) and ENSO-adjusted Niño1 + 2 (*x*-axis) indices in January 1979–December 2017. The closed triangles represent January 1982–December 1983 and January 1997–December 1998. The unit is °C. The correlations are 0.74 for all months, and 0.58 without January 1982–December 1983 and January 1997–December 1998

These distinctive evolution patterns are further displayed in longitude and time cross section Hovmöller analysis along the equator (Fig. 9). We note that 1983 and 1998 coastal El Niños formed after extreme basin-scale El Niño in 1982–1983 and 1997–1998, respectively (Fig. 9a, c), while 1987 and 2015 coastal El Niños occurred during basin-scale El Niños in 1986–1987 and 2014–2016, respectively (Fig. 9b, f). These coastal events are clearly linked to the evolution of basin scale atmospheric and oceanic variations. On the other hand, the coastal El Niños in 2008, 2014, and 2017 occurred after a strong La Niña or a moderate basin-wide cooling in the previous year (Figs. 8, 9d, e, g). These distinctive evolutions for the coastal El Niños imply different physical processes involved.

5.1 Coastal El Niños in 1983, 1987, and 1998

By comparing the composites between moderate El Niños and extreme (1982–1983 and 1997–1998) El Niños in both observations and models, Lengaigne and Vecchi (2010) noted that meridional migration of ITCZ not only preconditions the termination of El Niños in general, but also leads to a peculiar termination of the extreme El Niños. For the extreme (1982–1983, 1997–1998) and strong (1986–1987) basin-scale El Niño events (see Fig. 10), an equatorially centered ITCZ emerges in their decay phase and positive SSTAs in the eastern Pacific persist and strengthen well into the following boreal spring/early-summer. As a result, low-level wind convergence (or anomalous westerly wind) and SSTAs continue to reinforce each other in the eastern equatorial Pacific and along the west coast of South America. This seemed to be the main process that leads to coastal El Niños in 1983, 1987, and 1998 (Fig. 9a, b).

Specifically, the ITCZ (as depicted by the averaged OLR in 100°–80°W) is along 5°N before November 1982, November 1986, and November 1997 (Figs. 10a, c, e). Following its seasonal progression, it subsequently shifts southward towards the equator. Correspondingly, the positive SSTAs first decay, then persist or strengthen. Consistent with Lengaigne and Vecchi (2010), extreme El Niños are accompanied by anomalously strong convection in the eastern tropical Pacific (see contours in Fig. 10a, c, e) that leads to the convergence of the trade winds in the region and suppression of wind-forced upwelling (Fig. 10b, d, f). It is noted that the anomalous downwelling (negative values of vertical velocity, shown as shading in Fig. 10b, d, f) is present before January or February, and then anomalous westerly winds are observed. As a result of the anomalous downwelling and westerly winds (Fig. 10b, d, f), the thermocline (represented by D20; contours in Fig. 10b, d, f) deepens and positive D20 anomalies persist. Thus, the warming in the eastern tropical Pacific following extreme El Niño years can persist into boreal spring or even in summer, leading to a coastal El Niño. It should be pointed out that the basin-scale El Niño in 2015–2016 had comparable intensity with that in 1982–1983 and 1997–1998 (Huang et al. 2016), but no coastal El Niño happened in 2016 following this extreme event. That may imply that additional factor(s) also play a

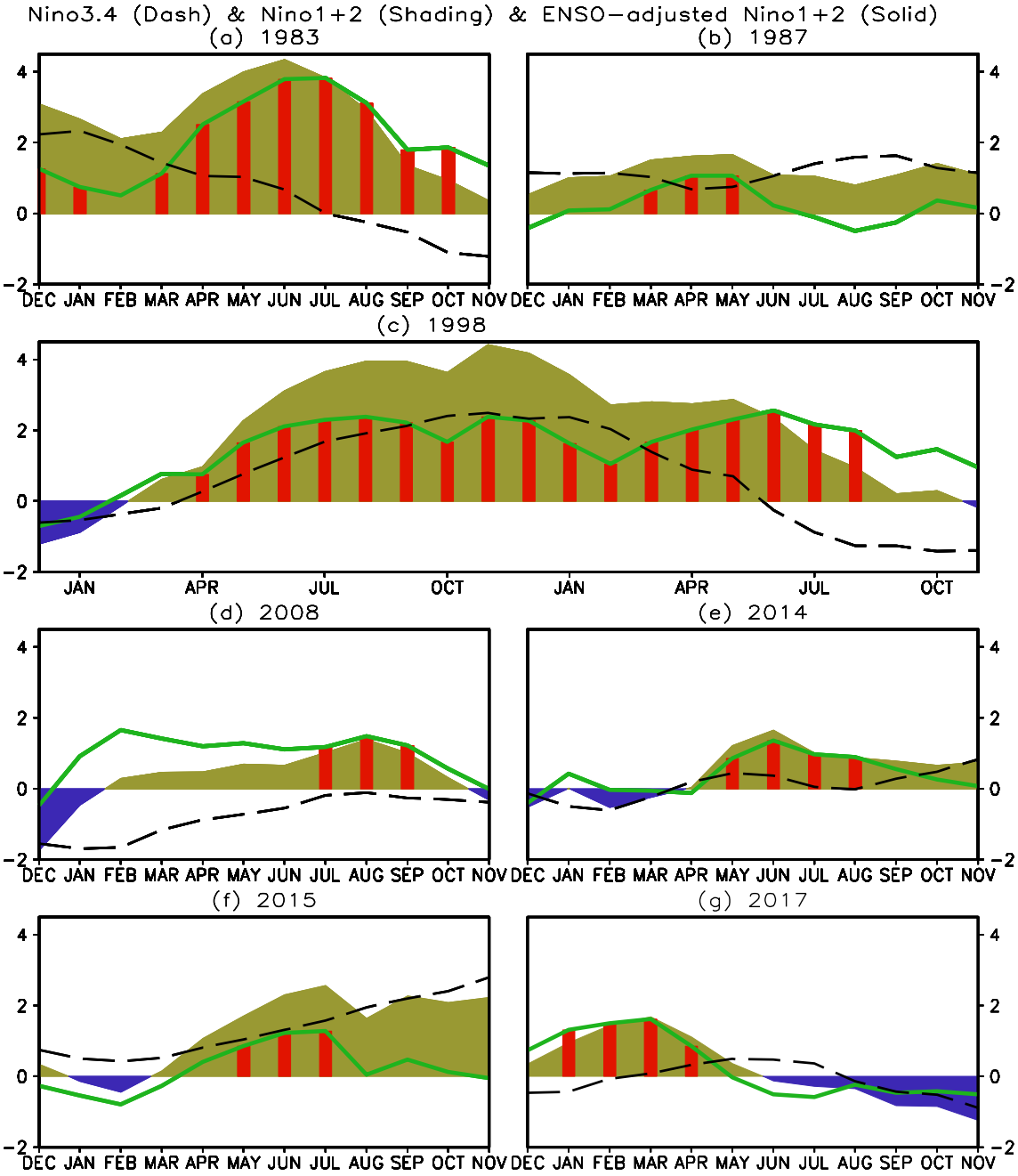

Fig. 8 Evolution of 3-month running mean Niño1+2 (shading), ENSO-adjusted Niño1+2 (green solid line), and Niño3.4 (dashed line) indices in the seven coastal Niño events. The bars represent the months that both the Niño1+2 index is equal to or larger than one STD (0.8 °C) and the ENSO-adjusted Niño1+2 index is equal to or larger than one STD (0.6 °C). The unit is °C

role in determining if there is a follow-up coastal El Niño after an extreme/strong basin-scale El Niño.

5.2 Coastal El Niños in 2014 and 2015

For the formation of the coastal El Niños in 2014 and 2015, we note that westerly wind bursts (WWBs) in the central-west equatorial Pacific may play an important role. In 2014, there were two WWBs in late January and late February (shading, top panel of Fig. 11a), while in 2015, multiple weak WWBs were evident in the first half of the years (shading, bottom panel of Fig. 11a). These WWBs triggered downwelling Kelvin waves (contour, Fig. 11a) that suppressed upwelling in the far eastern equatorial Pacific (shading in Fig. 11b; see also McPhaden 2015). These Kelvin waves caused warming in the Niño1+2 region a few

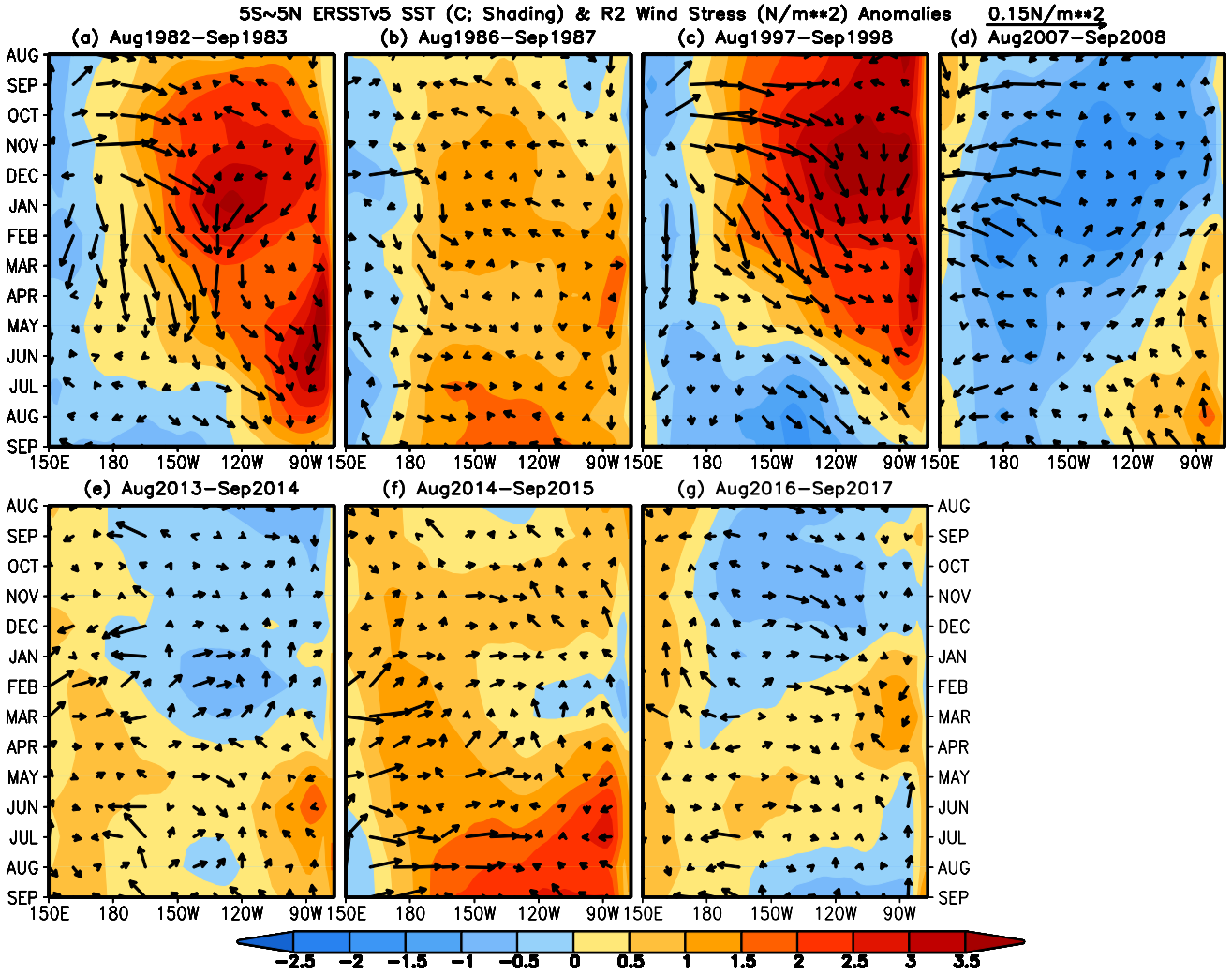

Fig. 9 Time and longitude evolution of monthly mean SST (shading), and wind stress (vector) anomalies averaged in 5°S–5°N during **a** August 1982–September 1983, **b** August 1986–September 1987, **c** August 1997–September 1998, **d** August 2007–September 2008, **e** August 2013–September 2014, **f** August 2014–September 2015, and **g** August 2016–September 2017. The unit is °C for SST and N/m^2 for wind stress

months later (Fig. 9, contour in Fig. 11b), leading to the formation of the coastal El Niños in 2014 and 2015. McPhaden et al. (2015) also noted that remotely forced Kelvin waves in late 1974 and early 1975 triggered a brief and weak coastal El Niño in 1975 (see their Fig. 3).

Such a mechanism is similar to that of basin-scale El Niños dominated by the Bjerknes feedback (Bjerknes 1969). The feedback involves anomalous zonal SST gradients, surface wind stress anomalies, and thermocline depth fluctuations that are triggered by WWBs and associated downwelling Kelvin waves. For the coastal El Niño event in 2015, it evolved into an extreme basin-scale El Niño in 2015–2016 (Huang et al. 2016; L'Heureux et al. 2017). Nevertheless, it is unclear why such strong WWBs and eastward propagation of a Kelvin wave in 2014 just triggered a coastal El Niño instead of a basin-scale El Niño, though both Levine and McPhaden (2016) and Tseng et al. (2017) argued that formation of a basin-scale El Niño needs multiple WWBs. Nevertheless, this may imply that even with strong subsurface warming, lack of multiple/persistent WWBs (Menkes et al. 2014) and/or the presence of the easterly wind events (Hu and Fedorov 2016) may halt a basin-scale El Niño development, like in 2014.

5.3 Coastal El Niños in 2008, and 2017

Unlike the coastal El Niños in 1983, 1987, 1998, 2014, and 2015, for the coastal El Niños in 2008 and 2017, there is no evidence that they were connected with extreme basin-scale El Niños or eastward propagation of downwelling Kelvin waves (not shown). This is consistent with Takahashi and Martínez (2018) who noted that downwelling equatorial

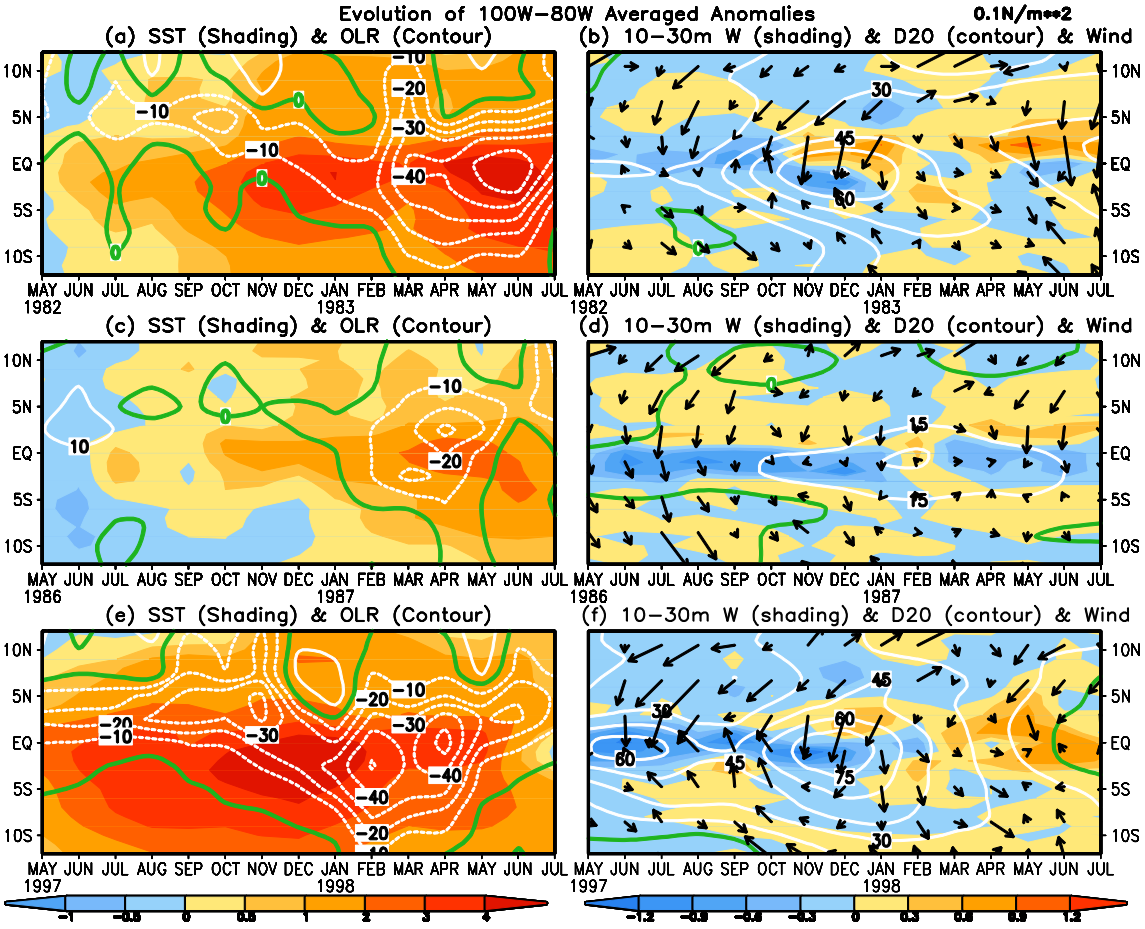

Fig. 10 Time and latitude evolution of monthly mean **a, c, e** SST (shading) and OLR (contour), **b, d, f** vertical velocity (10–30 m average; shading), D20 (contour), and surface wind stress (vector) anomalies averaged in 100°−80°W during **a, b** May 1982–July 1983, **c, d** May 1986–July 1987, and **e, f** May 1997–July 1998. The unit is °C for SST, W/m^2 for OLR, mm/s for vertical velocity, m for D20, and N/m^2 for wind stress. The contour interval is 10 W/m^2 for OLR and 15 m for D20, and the zero contour is bold green

waves played little role in the initiation of a very strong coastal El Niño in 1925. The coastal warming in 2008 and 2017 occurred during or slightly after the warm phase of the seasonal cycle in the eastern tropical Pacific (Fig. 12). Such warming was accompanied by westerly surface wind anomalies to the west, such as in the average between 100°–160°W (Fig. 12), before the warm peak, with easterly wind anomalies emerging after the warm peak. This implies an anomalous seasonal weakening of the trade winds that trigger the coastal responses, consistent with Garreaud (2018). Garreaud (2018) proposed that a remotely forced, sustained weakening of free tropospheric westerly flow impinging on the subtropical Andes lead to a relaxation of the southeasterly trades off the coast in the spring of 2017, which in turn warmed the eastern Pacific through the weakening of upwelling in a near-coastal band and the reduction of the evaporative cooling farther offshore. Different from 1925 coastal El Niño (Takahashi and Martínez 2018), it seems that the meridional component of the surface wind didn't play a dominant role in these two more recent coastal El Niños. Takahashi and Martínez (2018) argued that an abrupt onset of strong northerly winds across the equator played an important role for the coastal warming in 1925. For the 2008 and 2017 events, the westerly wind anomalies resulted in anomalous convergence in the eastern Pacific in boreal winter and spring with anomalous warming that enhanced and extended the warm phase in the seasonal cycle, thus favoring the development of a coastal El Niño (shading and contours in Fig. 12a, b). From Fig. 12c, d, we note that the surface heat flux played a dominant role while thermocline depth fluctuations (D20) likely played a secondary role in generating coastal warming in 2008 and 2017.

To some extent, the mechanism discussed above may be analogous to the formation of the Benguela warm events in the tropical Atlantic proposed by Hirst and Hastenrath (1983), Hu and Huang (2007), and Lübbecke et al. (2010). They suggested a causal chain of ocean–atmosphere anomalies in the equatorial Atlantic Ocean and the Angola coast.

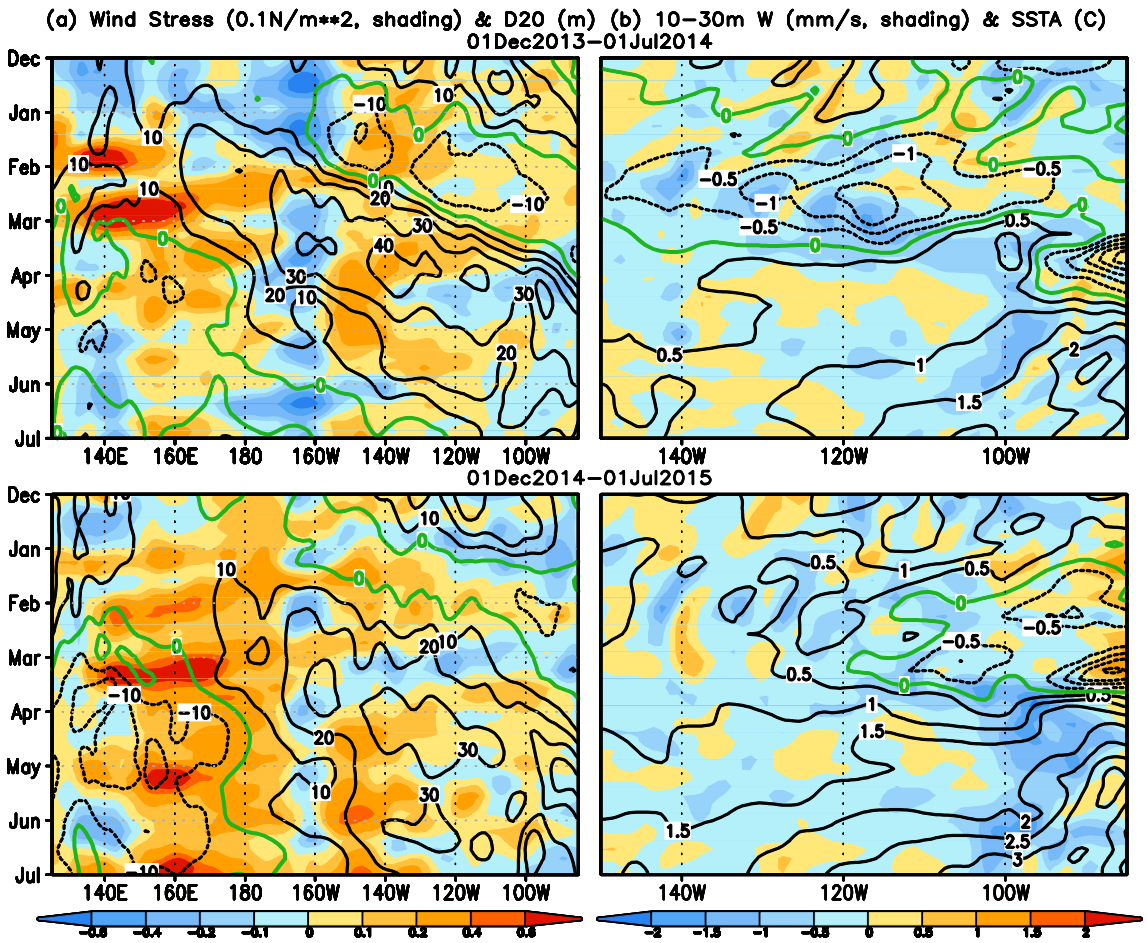

Fig. 11 Time and longitude evolution of pentad mean **a** zonal component of surface wind stress (shading) and D20 (contour), and **b** vertical velocity (10–30 m average; shading) and SST (contour) anomalies averaged in 2°S–2°N during 01 December 2013–01 July 2014 (top panel) and 01 December 2014–01 July 2015 (bottom panel). The unit is N/m^2 for wind stress, m for D20, mm/s for vertical velocity, and °C for SST

Anomalous seasonal relaxation of the easterly wind stress over the western equatorial Atlantic remotely generates positive SST departures in the eastern South Atlantic (along the Angola coast), a large relaxation being followed by the positive SST anomalies. Given the zonal extent of the Atlantic, which is about one-third of the Pacific, the spatial pattern of the wind-SST connection described by Hirst and Hastenrath (1983) for the whole domain of the tropical Atlantic is of the comparable zonal extent as the spatial scale of processes depicted in Fig. 12. Specifically, the patterns of the mean surface wind, SST and ITCZ, as well as their seasonal cycle, bear similarity between these two ocean basins. Therefore, the equatorial westerly wind anomalies present during these events confined in the eastern Pacific are unlikely generated by the zonal shift of convection near the warm pool, as in basin-scale El Niños. Instead, like Bengula warm events in the tropical Atlantic, these wind anomalies are possibly related to an abnormal seasonal change in the trade winds and the ITCZ in the central and eastern equatorial Pacific during late boreal fall and winter (see for example Zhang and McPhaden 2006, 2008). In this sense, the coastal El Niños in 1983, 1987, 1997, 2008, and 2017 are more exclusively generated within the cold tongue-ITCZ-trade wind complex.

In addition to the diversity of coastal El Niños in their intensity, duration, evolution and associated physical processes, their impacts on regional climate vary. For example, precipitation in tropical South America (shading over the land in Fig. 13) was mainly above average during coastal El Niños in 2008 and 2017 (Fig. 13d, g) but below normal in 1987 (Fig. 13b). Both negative and positive precipitation anomalies were present during the coastal El Niños in 1998, 2014, and 2015 (Fig. 13c, e, f). Though rainfall was mostly below normal through much of 1982–1983 along the west coast of South America, excessive rains in March–May 1983 (Fig. 13a) were devastating. Such diversity of impacts may imply that in addition to the SSTAs (shading over the ocean in Fig. 13) combined with the effect with the seasonal cycle (contour in Fig. 13), some other factors, such as extratropical

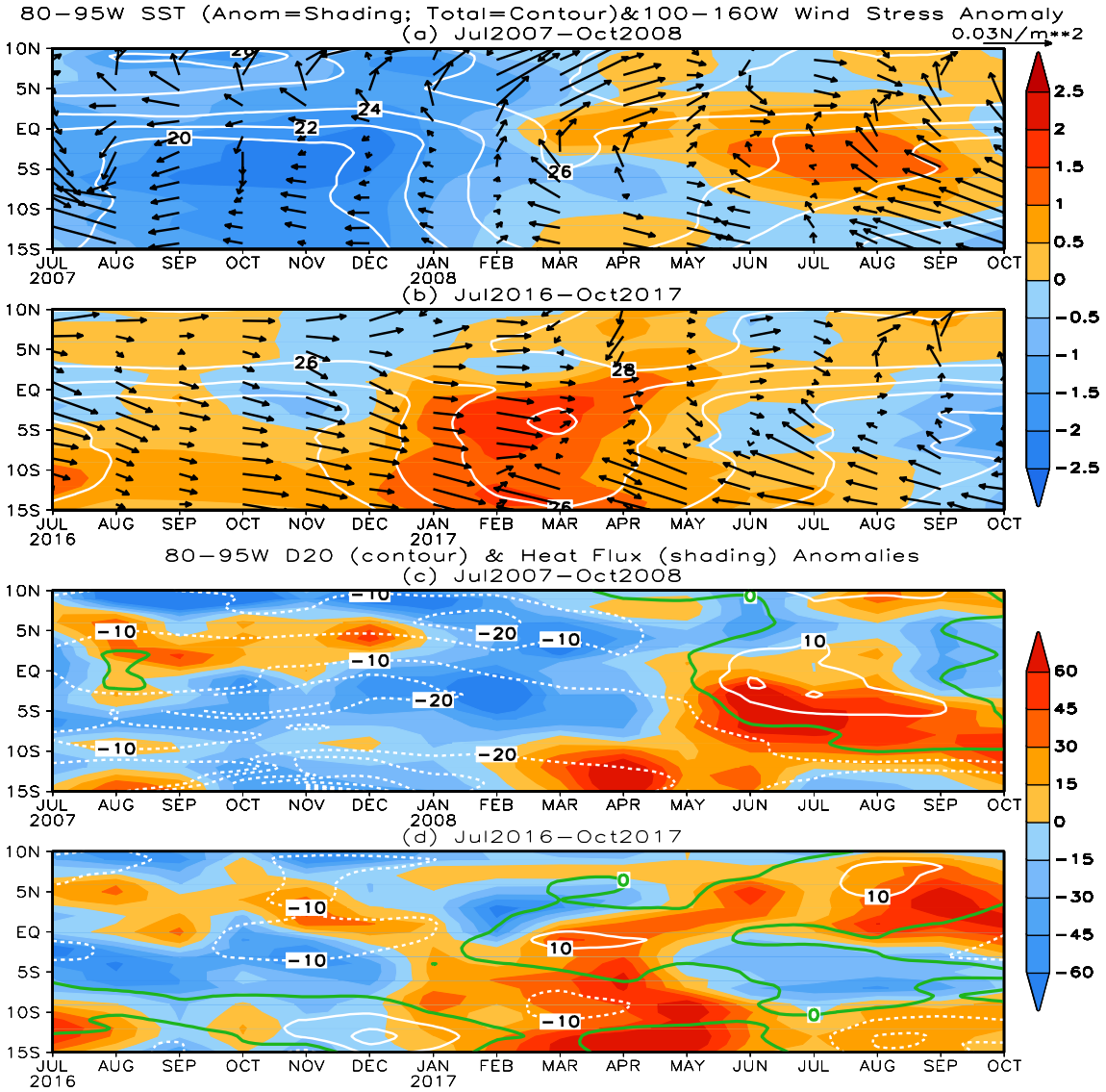

Fig. 12 Time and latitude evolution of monthly mean SST (contour) and SSTA averaged in 80°–95°W (shading), and wind stress anomaly averaged in 100°–160°W (vector) during **a** July 2007–October 2008, **b** July 2016–October 2017; and time and latitude evolution of monthly mean D20 (contour) and surface heat flux (shading) anomalies averaged in 80°–95°W during **c** July 2007–October 2008, **d** July 2016–October 2017. Downward (upward) heat flux is positive (negative). The unit is °C for SST and SSTA, N/m^2 for wind stress, m for D20, and W/m^2 for heat flux

systems and internal dynamical processes, may have a crucial influence.

6 Summary and discussion

The catastrophic impact of coastal El Niños on life and property as well as limited knowledge about the physics behind such events motivated this study. This work first examined the connection between SSTAs in the central and far-eastern equatorial Pacific on both seasonal and interdecadal time scales. Then, criteria were proposed to identify coastal El Niños, and the various possible mechanisms of generating coastal El Niños were examined.

Coastal El Niño and basin-scale El Niño occur together most of the time so that Niño3.4 and Niño1 + 2 indices are positively correlated, implying that the variations of SSTAs in the central and far-eastern equatorial Pacific are largely coherent. For the entire record (1854–2017), the maximum correlation occurs when the Niño3.4 index lags the Niño1 + 2 index by 1–2 months, suggesting that SST variations in the far-eastern equatorial Pacific occur slightly earlier than that in the central equatorial Pacific. However, for shorter segments of the record, the lead-lag relationship

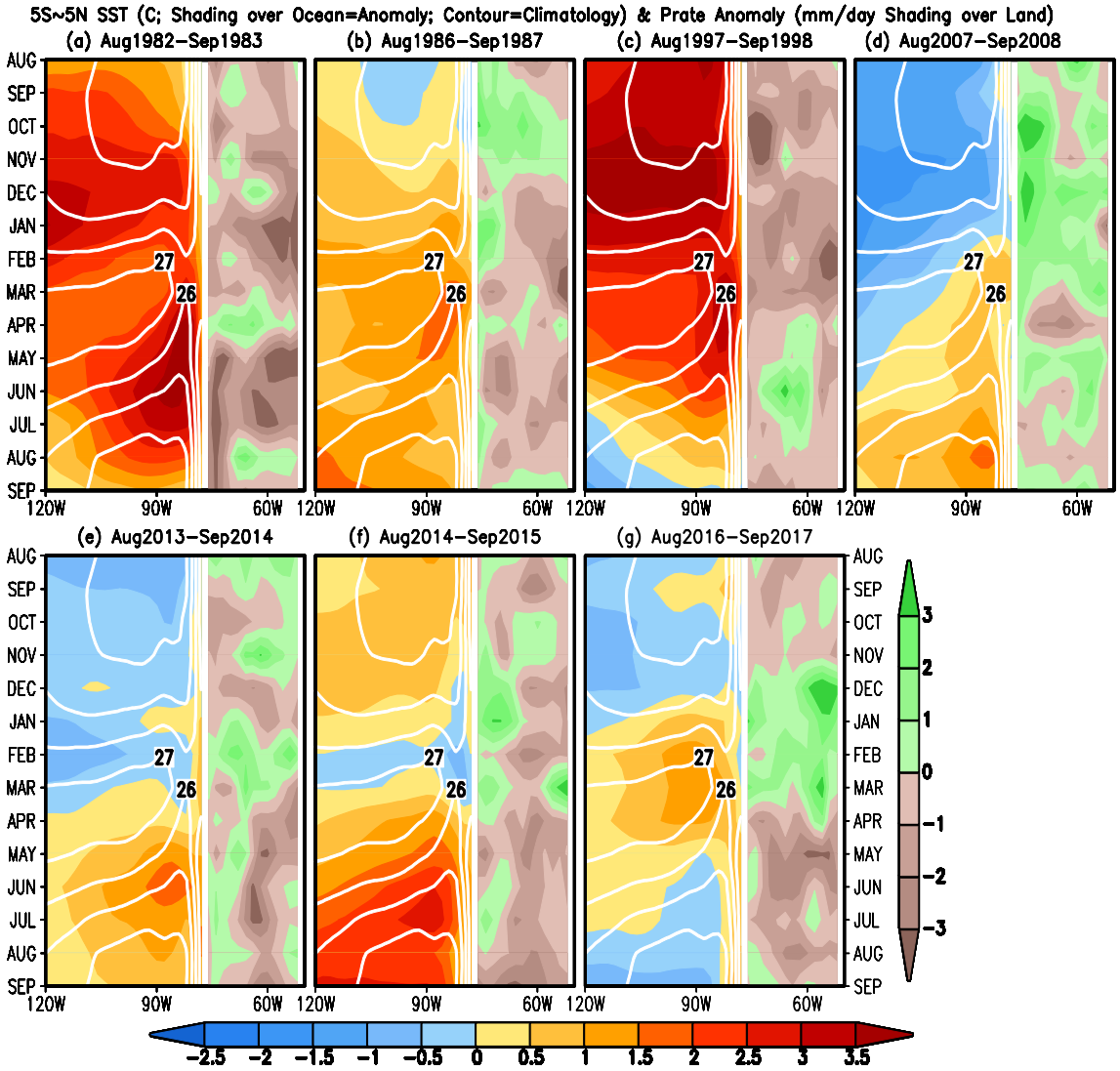

Fig. 13 Time and longitude evolution of monthly mean SST anomaly (shading), SST climatology (contours), and precipitation anomaly over the adjacent land averaged in 5°S–5°N during **a** August 1982–September 1983, **b** August 1986–September 1987, **c** August 1997–September 1998, **d** August 2007–September 2008, **e** August 2013–September 2014, **f** August 2014–September 2015, and **g** August 2016–September 2017. The unit is °C for SST and mm/day for precipitation

varies. For example, the Niño3.4 index lags the Niño1 + 2 index by 1–3 months during 1870–1980 (a period of pronounced westward propagation of anomalies), while the maximum lead-lag correlations occurred at 0-month lead-lag after about 1980, suggesting a change of zonal propagation direction of SSTAs associated with El Niño after 1980 (Wang 1995; McPhaden and Zhang 2009). Also, the correlations are relatively stronger during 1875–1915 and since 1960, and weaker during 1920–1960. Interestingly, the lead-lag anomaly correlations vary with calendar month. For instance, from late boreal spring to winter, the lead time of the Niño1 + 2 index to the Niño3.4 index reduces from 7 to 8 months to 0 month, suggesting that the westward propagation of the SSTA along the equator occurs only in the development phases of ENSO.

In addition to coastal El Niños which occur simultaneously with basin-scale El Niño, there are also coastal El Niños with warming concentrated in the southeastern coastal region. In this work, we define such type of coastal El Niño event when both the 3-month mean Niño1 + 2 and ENSO-adjusted Niño1 + 2 indices are equal to or larger than one STD (0.8 °C, 0.6 °C) and they also persist for at least three consecutive overlapping seasons. According to this definition, there were seven coastal El Niño events during 1979–2017: 1983, 1987, 1998, 2008, 2014, 2015, and 2017. These coastal El Niños are driven by different mechanisms.

For the coastal El Niños in 1983, 1987, and 1998, which occurred subsequent to the extreme/strong El Niños in 1982–1983, 1986–1987, and 1997–1998 respectively, an equatorially centered ITCZ emerged during the decay phase and positive SSTAs in the eastern Pacific persisted and strengthened well into boreal spring/early-summer. As a result, a coastal El Niño formed. This mechanism is similar to that proposed by Lengaigne and Vecchi (2010) to explain the long persistence and even enhancement of the SSTAs in the eastern Pacific in the late stage of extreme El Niños. They argued that the extreme El Niños are accompanied by anomalously strong convection in the eastern tropical Pacific, leading to the relaxation of the trade winds in the region and suppression of wind-forced upwelling, resulting in warming in the eastern tropical Pacific.

The mechanism for coastal El Niño events in 2014 and 2015 are similar to that for basin-scale El Niños. These two coastal El Niños were associated with thermocline fluctuation driven by eastward propagation of a downwelling Kelvin wave that was triggered by westerly wind bursts.

Unlike the coastal El Niños in 1983, 1987, 1998, 2014, and 2015, the coastal El Niños in 2008 and 2017 were not connected with extreme/strong basin-scale El Niño or eastward propagation of downwelling Kelvin waves, instead they were associated with westerly surface wind anomalies in the eastern equatorial Pacific and largely driven by ocean surface heat flux. The westerly wind anomalies resulted in anomalous convergence and anomalous warming in the eastern Pacific in boreal winter and spring that enhanced the seasonal cycle or extended the warm phase of the seasonal cycle, thus forming a coastal El Niño.

In this analysis we note the caveat that short data record (1979–2017) may not cover the full range of possible coastal El Niño types. Nevertheless, the results here clearly demonstrate a wide variety of costal warming events, including their duration, evolution, and mechanisms. Also, in this work, we only examine coastal warm events, but not cold events. From Figs. 5 and 6, we see that the SSTAs on the cold side never get as large as on the warm side. Such amplitude asymmetry between coastal El Niño and La Niña may be because after the thermocline outcrops, SSTs can't go down any further. In the future, we plan to investigate the corresponding cold events to identify their evolution, as well as the similarities and differences in their associated physical processes compared to coastal El Niños. We also plan to study the predictability and prediction skill of coastal ENSOs based on seasonal prediction data sets, e.g., North American Multi-Model Ensemble (Kirtman et al. 2014; Kumar et al. 2017).

Acknowledgements The authors thank reviewers for their constructive comments and insightful suggestions. The scientific results and conclusions, as well as any view or opinions expressed herein, are those of the authors and do not necessarily reflect the views of NWS, NOAA, or the Department of Commerce. This is PMEL Contribution No. 4736. B. Huang is supported by Grants from NSF (AGS-1338427), NASA (NNX14AM19G), NOAA (NA14OAR4310160 and NA17OAR4310144).

References

An S-I, Jin F-F (2004) Why El Niño is stronger than La Niña. J Clim 17(12):2399–2412

Ashok K, Behera SK, Rao SA, Weng H, Yamagata T (2007) El Niño Modoki and its possible teleconnection. J Geophys Res 112:C11007. https://doi.org/10.1029/2006JC003798

Behringer DW (2005) The global ocean data assimilation system (GODAS) at NCEP. 11th symposium on integrated observing and assimilation systems for the atmosphere, oceans, and land surface (IOAS-AOLS), San Antonio, TX, Am. Meteor. Soc. 3.3 [Available online at https://ams.confex.com/ams/87ANNUAL/webprogram/11IOAS.html]

Bjerknes J (1969) Atmospheric teleconnections from the equatorial Pacific. Mon Weather Rev 97:163–172

Capotondi A et al (2015) Understanding ENSO diversity. Bull Am Meteorol Soc 96:921–938

D'Arrigo R, Cook ER, Wilson RJ, Allan R, Mann ME (2005) On the variability of ENSO over the past six centuries. Geophys Res Lett 32:03711

Davey MK, Brookshaw A, Ineson S (2014) The probability of the impact of ENSO on precipitation and near-surface temperature. Clim Risk Manag 1:5–24

Deser C, Wallace JM (1987) El Niño events and their relation to the Southern Oscillation: 1925–1986. J Geophys Res 92:14189–14196

Frase B (2017) Peru's floods teach tough lessons. Nature 544:405–406

Garreaud RD (2018) A plausible atmospheric trigger for the 2017 coastal El Niño. Int J Climatol. 38(S1):e1296–e1302. https://doi.org/10.1002/joc.5426

Hirst A, Hastenrath S (1983) Atmosphere–ocean mechanisms of climate anomalies in the Angola–tropical Atlantic sector. J Phys Oceanogr 13:1146–1157

Hoerling M, Kumar A, Zhong M (1997) El Niño, La Niña, and the nonlinearity of their teleconnections. J Clim 10:1769–1786

Hu S, Edorov AF (2016) Exceptionally strong easterly wind burst stalling El Niño of 2014. Proc Natl Acad Sci 113:2005–2010

Hu Z-Z, Huang B (2007) Physical processes associated with tropical Atlantic SST gradient during the anomalous evolution in the southeastern ocean. J Clim 20(14):3366–3378

Hu Z-Z, Kumar A, Jha B, Wang W, Huang B, Huang B (2012) An analysis of warm pool and cold tongue El Niños: air–sea coupling processes, global influences, and recent trends. Clim Dyn 38(9–10):2017–2035. https://doi.org/10.1007/s00382-011-1224-9

Hu Z-Z, Kumar A, Xue Y, Jha B (2014) Why were some La Niñas followed by another La. Niña? Clim Dyn 42(3–4):1029–1042. https://doi.org/10.1007/s00382-013-1917-3

Hu Z-Z, Kumar A, Huang B, Zhu J, Zhang R-H, Jin F-F (2017) Asymmetric evolution of El Niño and La Niña: the recharge/discharge processes and role of the off-equatorial sea surface height anomaly. Clim Dyn 49(7–8):2737–2748. https://doi.org/10.1007/s00382-016-3498-4

Huang B, L'Heureux M, Hu Z-Z, Zhang H-M (2016) Ranking the strongest ENSOs while incorporating SST uncertainty. Geophys Res Lett 43(17):9165–9172. https://doi.org/10.1002/2016GL070888

Huang B, Thorne PW, Banzon VF, Boyer T, Chepurin G, Lawrimore JH, Menne MJ, Smith TM, Vose RS, Zhang H-M (2017) Extended reconstructed sea surface temperature version 5 (ERSSTv5), upgrades, validations, and intercomparisons. J Clim 30(20):8179–8205. https://doi.org/10.1175/JCLI-D-16-0836.1

Jin F-F, An S, Timmermann A, Zhao J (2003) Strong El Niño events and nonlinear dynamical heating. Geophys Res Lett 30(3):1120. https://doi.org/10.1029/2002GL016356

Kanamitsu M, Ebisuzaki W, Woollen J, Yang S-K, Hnilo JJ, Fiorino M, Potter GL (2002) NCEP-DOE AMIP-II reanalysis (R-2). Bull Am Meteorol Soc 83:1631–1643. https://doi.org/10.1175/BAMS-83-11-1631

Kao H-Y, Yu J-Y (2009) Contrasting eastern-Pacific and central-Pacific types of ENSO. J Clim 22:615–632

Kirtman BP et al (2014) The North American multimodel ensemble: phase-1 seasonal-to-interannual prediction; phase-2 toward developing intraseasonal prediction. Bull Am Meteorl Soc 95:585–601

Kug J-S, Jin F-F, An S-I (2009) Two types of El Niño events: cold tongue El Niño and warm pool El Niño. J Clim 22:1499–1515. https://doi.org/10.1175/2008JCLI2624.1

Kumar A, Hoerling MP (1997) Interpretation and implications of observed inter-El Niño variability. J Clim 10:83–91

Kumar A, Hu Z-Z, Jha B, Peng P (2017) Estimating ENSO predictability based on multi-model hindcasts. Clim Dyn 48(1–2):39–51. https://doi.org/10.1007/s00382-016-3060-4

L'Heureux M, Takahashi K, Watkins A, Barnston A, Becker E, Di Liberto T, Gamble F, Gottschalck J, Halpert M, Huang B, Mosquera-Vásquez K, Wittenberg A (2017) Observing and predicting the 2015–2016 El Niño. Bull Am Meteor Soc 98(7):1363–1382. https://doi.org/10.1175/BAMS-D-16-0009.1

Larkin NK, Harrison DE (2005) Global seasonal temperature and precipitation anomalies during El Niño autumn and winter. Geophys Res Lett 32:L13705. https://doi.org/10.1029/2005GL022738

Lengaigne M, Vecchi GA (2010) Contrasting the termination of moderate and extreme El Niño events in coupled general circulation models. Clim Dyn 35:299–313. https://doi.org/10.1007/s00382-009-0562-3

Levine AFZ, McPhaden MJ (2016) How the july 2014 easterly wind burst gave the 2015-6 El Niño a head start. Geophys Res Lett 43:6503–6510. https://doi.org/10.1002/2016GL069204

Liebmann B, Smith CA (1996) Description of a complete (interpolated) outgoing long wave radiation dataset. Bull Am Meteor Soc 77:1275–1277

Lübbecke JF, Böning CW, Keenlyside NS, Xie S-P (2010) On the connection between Benguela and equatorial Atlantic Niños and the role of the South Atlantic Anticyclone. J Geophys Res 115:C09015. https://doi.org/10.1029/2009JC005964

McPhaden MJ (2012) A 21st century shift in the relationship between ENSO SST anomalies and upper ocean heat content. Geophys Res Lett 39(9):L09706. https://doi.org/10.1029/2012GL051826

McPhaden MJ, Zhang X (2009) Asymmetry in zonal phase propagation of ENSO sea surface temperature anomalies. Geophys Res Lett 36:L13703. https://doi.org/10.1029/2009GL038774

McPhaden MJ, Zebiak SE, Glantz MH (2006) ENSO as an integrating concept in Earth science. Science 314:1740–1745

McPhaden MJ, Timmermann A, Widlansky MJ, Balmaseda MA, Stockdale TN (2015) The curious case of the El Niño that never happened: a perspective from 40 years of progress in climate research and forecasting. Bull Am Meteorol Soc 96(10):1647–1665. https://doi.org/10.1175/BAMS-D-14-00089.1

Menkes CE, Lengaigne M, Vialard J, Puy M, Marchesiello P, Cravatte S, Cambon G (2014) About the role of westerly wind events in the possible development of an El Niño in 2014. Geophys Res Lett 41:6476–6483

National Research Council (2010) Assessment of intraseasonal to interannual climate prediction and predictability. the National Academies Press, Washington, p192 (**ISBN-10: 0-309-15183-X**)

Philander SGH (1990) El Niño, La Niña and the Southern Oscillation, ISBN 0125532350. Academic Press, San Diego, p 293

Rasmusson EM, Carpenter TH (1982) Variation in tropical sea surface temperature and surface wind fields associated with Southern Oscillation/El Niño. Mon Weather Rev 110:354–384

Rasmusson EM, Wallace JM (1983) Meteorological aspects of the El Niño/Southern Oscillation. Science 222:1195–2202

Sanabria J, Bourrel L, Dewitte B, Frappart F, Rau P, Solis O, Labat D (2018) Rainfall along the coast of Peru during strong El Niño events. Int J Climatol 38(4):1737–1747. https://doi.org/10.1002/joc.5292

Sarachik ES, Cane MA (2010) The El Niño-Southern oscillation phenomenon. Cambridge University Press, London, p 384

Takahashi K, Martínez AG (2018) The very strong coastal El Niño in 1925 in the far-eastern Pacific. Clim Dyn. https://doi.org/10.1007/s00382-017-3702-1

Tseng Y-H, Hu Z-Z, Ding R-Q, Chen H-C (2017) An ENSO prediction approach based on ocean conditions. Clim Dyn 48(5–6):2025–2044. https://doi.org/10.1007/s00382-016-3188-2

Wang B (1995) Interdecadal changes in El Niño onset in the last four decades. J Climate 8:267–285

Wang X, Tan W, Wang C (2018) A new index for identifying different types of El Niño Modoki events. Clim Dyn 50(7–8):2753–2765. https://doi.org/10.1007/s00382-017-3769-8

Wyrtki K (1975) El Niño-The dynamic response of the equatorial Pacific Ocean to atmospheric forcing. J Phys Oceanogr 5:572–584

Xie P, Arkin PA (1997) Global precipitation: a 17-year monthly analysis based on gauge observations, satellite estimates, and numerical model outputs. Bull Am Meteorol Soc 78:2539–2558

Yu J-Y, Kim ST (2011) Reversed spatial asymmetries between El Niño and La Niña and their linkage to decadal ENSO modulation in CMIP3 models. J Clim 24:5423–5434. https://doi.org/10.1175/JCLI-D-11-00024.1

Zhang X, McPhaden MJ (2006) Wind stress variations and interannual sea surface temperature anomalies in the eastern equatorial Pacific. J Clim 19:226–241

Zhang X, McPhaden MJ (2008) Eastern equatorial Pacific forcing of ENSO sea surface temperature anomalies. J Clim 21:6070–6079

Zhang W-J, Li J-P, Jin F-F (2009) Spatial and temporal features of ENSO meridional scales. Geophys Res Lett 36:L15605. https://doi.org/10.1029/2009GL038672

Zhu J, Zhou G-Q, Zhang R-H, Sun Z (2011) On the role of oceanic entrainment temperature (T_e) in decadal changes of El Niño/Southern Oscillation. Ann Geophys 29:529–540. https://doi.org/10.5194/angeo-29-529-2011